

Facile Synthesis and Enhanced Intermediate Temperature Electrical Properties of Novel $\text{Sn}_{0.9}\text{Mg}_{0.1}\text{P}_2\text{O}_7/\text{KSn}_2(\text{PO}_4)_3$ Composite Electrolyte

Junlong Liu, Ruifeng Du, Ruijuan Shi*, Hongtao Wang*

School of Chemical and Material Engineering, Fuyang Normal College; Anhui Provincial Key Laboratory for Degradation and Monitoring of Pollution of the Environment, Fuyang 236037, China

*E-mail: hongtaoking3@163.com, rjshi@foxmail.com

Received: 5 December 2017 / Accepted: 7 February 2018 / Published: 10 April 2018

The application of $\text{Sn}_{1-x}\text{M}_x\text{P}_2\text{O}_7$ electrolyte for solid oxide fuel cells is limited due to its poor sintering abilities. In this study, a new $\text{Sn}_{0.9}\text{Mg}_{0.1}\text{P}_2\text{O}_7/\text{KSn}_2(\text{PO}_4)_3$ composite electrolyte was facile synthesized and the structural and microstructural properties were characterized by XRD and SEM. These results exhibit that the $\text{Sn}_{0.9}\text{Mg}_{0.1}\text{P}_2\text{O}_7/\text{KSn}_2(\text{PO}_4)_3$ composite can be obtained by $\text{Sn}_{0.9}\text{Mg}_{0.1}\text{P}_2\text{O}_7$ *in-situ* reacted with inorganic melt salt. The electrical properties were tested using impedance spectroscopy in the range of 300 ~ 700 °C. The highest conductivity of $\text{Sn}_{0.9}\text{Mg}_{0.1}\text{P}_2\text{O}_7/\text{KSn}_2(\text{PO}_4)_3$ achieved was $6.3 \times 10^{-2} \text{ S} \cdot \text{cm}^{-1}$ in a dry nitrogen atmosphere at 700 °C. A H_2/O_2 fuel cell with a dense $\text{Sn}_{0.9}\text{Mg}_{0.1}\text{P}_2\text{O}_7/\text{KSn}_2(\text{PO}_4)_3$ electrolyte membrane was also constructed and achieved maximum power output densities of $47.2 \text{ mW} \cdot \text{cm}^{-2}$ and $130.9 \text{ mW} \cdot \text{cm}^{-2}$ at 600 °C and 700 °C, respectively.

Keywords: Composite electrolyte; Intermediate temperature fuel cell; Ceramics; Conductivity

1. INTRODUCTION

Yttria-stabilized zirconia (YSZ) is used in high-temperature solid oxide fuel cells (HT-SOFCs) because of its high stability and high ionic conductivity [1–2]. However, the most widely used electrolyte is limited by the high operating temperature which can lead to some complex influences on selecting electrodes, bonding materials and sealing materials at elevated temperatures. Therefore, many researchers have devoted their efforts to investigating the low-temperature (100 °C ~ 300 °C) and intermediate-temperature (300 °C ~ 700 °C) solid oxide fuel cells. And much research has reported that the performance of fuel cells can be enhanced through the modification of operation conditions (such as gas flow direction and gravity) and the development of new electrode materials,

cathode catalysts, and electrolytes [3–10]. As one of the most important factors, the electrolyte material plays a vital role in determining the performance of fuel cells.

In recent years, low-valence metal cations doped tin pyrophosphates, which possess high protonic conductivities at low temperature range (100 °C ~ 300 °C), have been applied in low-temperature solid oxide fuel cells (LT-SOFCs) [11–13]. However, $\text{Sn}_{1-x}\text{M}_x\text{P}_2\text{O}_7$ materials are still far from practical due to their poor sintering abilities. Composition is regarded as an extensively used and effective pathway to optimize the electrical properties of electrolytes for fuel cells. Hence, it becomes significant to design and synthesize dense and novel SnP_2O_7 -based composite electrolytes [14–17].

Recently, owing to their high ionic conductivity and high chemical stability, $(\text{K}/\text{Na})\text{M}_2(\text{PO}_4)_3$ ($\text{M} = \text{Sn}, \text{Ti}$) with a NASICON (Na Super Ionic Conductor) structure have received a great deal of attention as electrode materials for sodium-ion or lithium-ion batteries [18–21]. It is confirmed that chemical and thermal stability is a crucial factor for the application of electrolytes in fuel cells with a long-term performance. In our previous study, we explored the $\text{Sn}_{0.95}\text{Al}_{0.05}\text{P}_2\text{O}_7/\text{KSn}_2(\text{PO}_4)_3$ composite electrolyte and the results indicated that the $\text{Sn}_{0.95}\text{Al}_{0.05}\text{P}_2\text{O}_7$ and $\text{KSn}_2(\text{PO}_4)_3$ are fused together to form a dense composite [22]. It is necessary to find if $\text{KSn}_2(\text{PO}_4)_3$ can serve as a promoter for different R^{n+} -doped $\text{SnP}_2\text{O}_7/\text{KSn}_2(\text{PO}_4)_3$ composite electrolytes, and consequently to extend the applied temperature range to meet the demands of IT-SOFCs (300 °C ~ 700 °C).

In this work, we prepared other different metal ion doped SnP_2O_7 and a dense $\text{Sn}_{0.9}\text{Mg}_{0.1}\text{P}_2\text{O}_7/\text{KSn}_2(\text{PO}_4)_3$ composite electrolyte was also successfully fabricated in order to find the composite electrolyte with the best performance. The $\text{Sn}_{0.9}\text{Mg}_{0.1}\text{P}_2\text{O}_7/\text{KSn}_2(\text{PO}_4)_3$ composite was carefully examined by XRD and SEM. The conductivities and the performance in intermediate temperature fuel cells (ITFCs) of the $\text{Sn}_{0.9}\text{Mg}_{0.1}\text{P}_2\text{O}_7/\text{KSn}_2(\text{PO}_4)_3$ composite electrolyte were evaluated in detail.

2. EXPERIMENTAL

The $\text{Sn}_{0.9}\text{Mg}_{0.1}\text{P}_2\text{O}_7$ was prepared in a similar manner to our previously reported procedure [23]. In a typical process, 8.1373 g of SnO_2 and 0.2418 g of MgO were dispersed into 11.6 mL of H_3PO_4 (85 %) and heated at 350 °C for 1 h. Further heat treatment was performed at 600 °C for 2 h. After that, the resulting $\text{Sn}_{0.9}\text{Mg}_{0.1}\text{P}_2\text{O}_7$ powder and NaCl/KCl molten salt were fully mixed and reacted with each other at 650 °C for 1.5 h, giving the $\text{Sn}_{0.9}\text{Mg}_{0.1}\text{P}_2\text{O}_7/\text{KSn}_2(\text{PO}_4)_3$ sample. The obtained composite was milled and pressed at 200 MPa, and re-sintered at 650 °C for 1 h to obtain the $\text{Sn}_{0.9}\text{Mg}_{0.1}\text{P}_2\text{O}_7/\text{KSn}_2(\text{PO}_4)_3$ composite electrolyte (1.0 mm in thickness). The pure $\text{Sn}_{0.9}\text{Mg}_{0.1}\text{P}_2\text{O}_7$ pellet was also synthesized at 600 °C for 2 h as a reference.

X-ray powder diffraction (XRD) measurements of the $\text{Sn}_{0.9}\text{Mg}_{0.1}\text{P}_2\text{O}_7$ and the $\text{Sn}_{0.9}\text{Mg}_{0.1}\text{P}_2\text{O}_7/\text{KSn}_2(\text{PO}_4)_3$ composite were recorded on a X'Pert-pro MPD diffractometer using $\text{Cu K}\alpha$ radiation. Scanning electron microscopy (SEM) images of the $\text{Sn}_{0.9}\text{Mg}_{0.1}\text{P}_2\text{O}_7$ and the $\text{Sn}_{0.9}\text{Mg}_{0.1}\text{P}_2\text{O}_7/\text{KSn}_2(\text{PO}_4)_3$ composite were observed on a FEI Tecnai G2 F30 electron microscope.

In the conductivity measurement system, 20 %Pd-80 %Ag paste was used as the electrode and two Ag wires were used as current collectors. The conductivities of the $\text{Sn}_{0.9}\text{Mg}_{0.1}\text{P}_2\text{O}_7$ and the

$\text{Sn}_{0.9}\text{Mg}_{0.1}\text{P}_2\text{O}_7/\text{KSn}_2(\text{PO}_4)_3$ composite samples were determined by a CHI-660E electrochemical analyzer over the frequency range from 1 Hz to 10^6 Hz in a dry nitrogen atmosphere at 300 ~ 700 °C. An oxygen concentration discharge cell was constructed as: air, Pd-Ag | $\text{Sn}_{0.9}\text{Mg}_{0.1}\text{P}_2\text{O}_7/\text{KSn}_2(\text{PO}_4)_3$ | Pd-Ag, O_2 and the electromotive force was calculated to study the oxide ionic conduction under an oxygen-containing atmosphere at 700 °C. To evaluate the performance of $\text{Sn}_{0.9}\text{Mg}_{0.1}\text{P}_2\text{O}_7/\text{KSn}_2(\text{PO}_4)_3$ as an electrolyte for ITFCs, a H_2/O_2 fuel cell was constructed.

3. RESULTS AND DISCUSSION

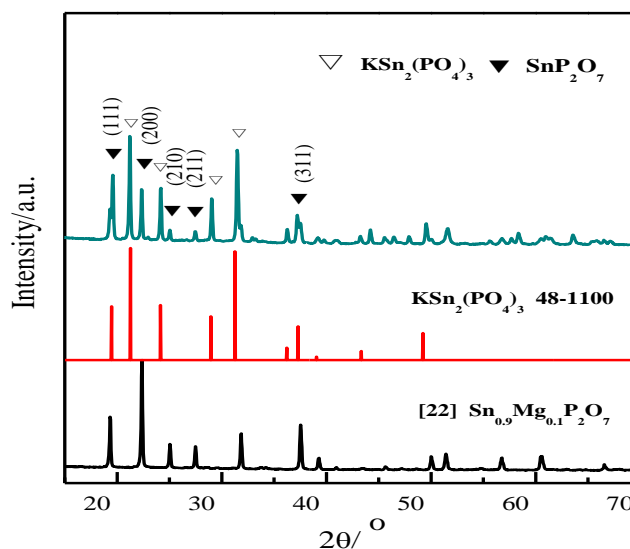


Figure 1. XRD patterns of $\text{Sn}_{0.9}\text{Mg}_{0.1}\text{P}_2\text{O}_7$ and $\text{Sn}_{0.9}\text{Mg}_{0.1}\text{P}_2\text{O}_7/\text{KSn}_2(\text{PO}_4)_3$ composite.

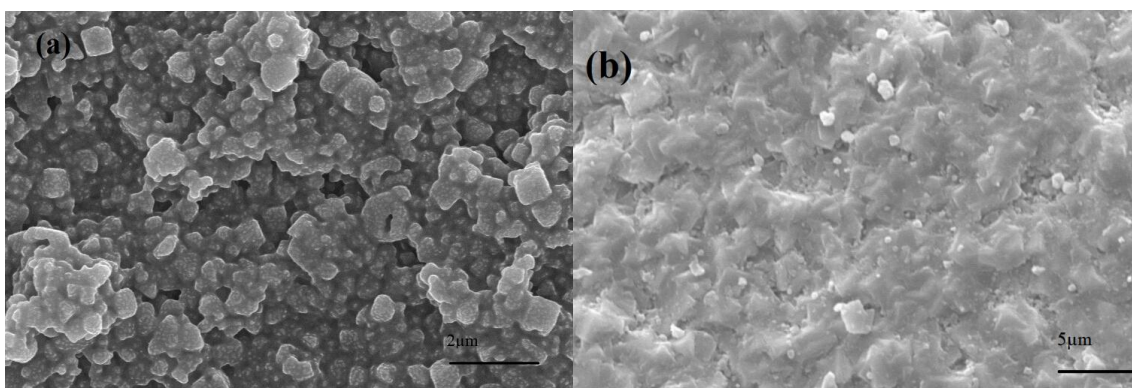


Figure 2. SEM images of external surfaces of $\text{Sn}_{0.9}\text{Mg}_{0.1}\text{P}_2\text{O}_7$ (a) and $\text{Sn}_{0.9}\text{Mg}_{0.1}\text{P}_2\text{O}_7/\text{KSn}_2(\text{PO}_4)_3$ (b).

Fig. 1 presents the XRD patterns of the $\text{Sn}_{0.9}\text{Mg}_{0.1}\text{P}_2\text{O}_7$ and $\text{Sn}_{0.9}\text{Mg}_{0.1}\text{P}_2\text{O}_7/\text{KSn}_2(\text{PO}_4)_3$ composite. Bare $\text{Sn}_{0.9}\text{Mg}_{0.1}\text{P}_2\text{O}_7$ showed typical diffraction peaks of cubic SnP_2O_7 phase (JCPDS 29-1352) and the diffraction angles (2θ) at 19.43°, 22.47°, 25.14°, 27.58° and 37.61° were ascribed to the

(111), (200), (210), (211) and (311) crystal planes of SnP_2O_7 , respectively [11,23]. The $\text{Sn}_{0.9}\text{Mg}_{0.1}\text{P}_2\text{O}_7/\text{KSn}_2(\text{PO}_4)_3$ composite exhibited characteristic diffraction peaks of cubic SnP_2O_7 phase (JCPDS 29-1352) and $\text{KSn}_2(\text{PO}_4)_3$ (JCPDS 48-1100) with a NASICON framework, and the diffraction angles (2θ) at 21.22° , 24.18° , 29.07° and 31.54° correspond to the (110), (113), (024) and (116) crystal planes of $\text{KSn}_2(\text{PO}_4)_3$, respectively. It is worth noting that all these diffraction peaks in $\text{Sn}_{0.9}\text{Mg}_{0.1}\text{P}_2\text{O}_7/\text{KSn}_2(\text{PO}_4)_3$ composite are consistent with SnP_2O_7 and $\text{KSn}_2(\text{PO}_4)_3$, implying that an *in-situ* reaction takes place between two closely contacted phases of $\text{Sn}_{0.9}\text{Mg}_{0.1}\text{P}_2\text{O}_7$ and inorganic melt salt during the calcination process and no impurities are formed.

Fig. 2 shows the SEM images of the $\text{Sn}_{0.9}\text{Mg}_{0.1}\text{P}_2\text{O}_7$ and $\text{Sn}_{0.9}\text{Mg}_{0.1}\text{P}_2\text{O}_7/\text{KSn}_2(\text{PO}_4)_3$ composite. As seen from Figure 2a, the $\text{Sn}_{0.9}\text{Mg}_{0.1}\text{P}_2\text{O}_7$ is composed of uniform cubic particles with particle size of 0.2-0.8 μm and exhibits a relatively dense microstructure. Figure 2b shows the morphology of the $\text{Sn}_{0.9}\text{Mg}_{0.1}\text{P}_2\text{O}_7/\text{KSn}_2(\text{PO}_4)_3$ composite. It can be observed that a fully dense and crack-free structure were formed, indicating that inorganic melt salt can act as a sintering aid and reactant for in situ formation of $\text{KSn}_2(\text{PO}_4)_3$ during the calcination procedure. The results demonstrate that modification of $\text{Sn}_{0.9}\text{Mg}_{0.1}\text{P}_2\text{O}_7$ with $\text{KSn}_2(\text{PO}_4)_3$ has great influence on the morphology of the $\text{Sn}_{0.9}\text{Mg}_{0.1}\text{P}_2\text{O}_7/\text{KSn}_2(\text{PO}_4)_3$ composite thus enhancing the densification, which might be helpful to ion transport.

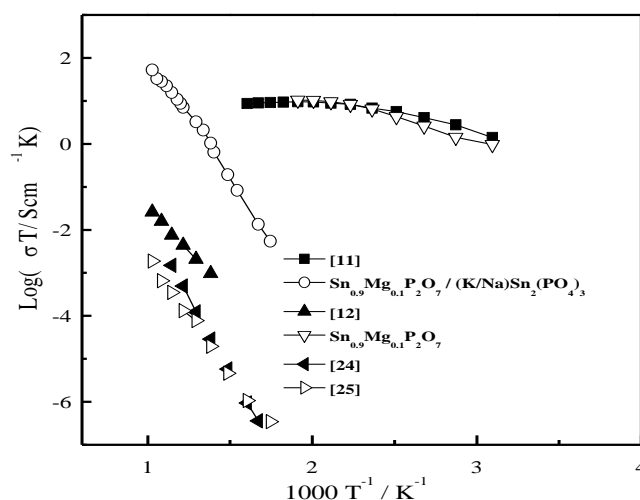


Figure 3. The $\log(\sigma T) \sim 1000 T^{-1}$ plots of $\text{Sn}_{0.9}\text{Mg}_{0.1}\text{P}_2\text{O}_7$ and $\text{Sn}_{0.9}\text{Mg}_{0.1}\text{P}_2\text{O}_7/\text{KSn}_2(\text{PO}_4)_3$ composite under dry nitrogen atmosphere.

The conductivities curves of the $\text{Sn}_{0.9}\text{Mg}_{0.1}\text{P}_2\text{O}_7$ electrolyte from 50°C to 250°C and the $\text{Sn}_{0.9}\text{Mg}_{0.1}\text{P}_2\text{O}_7/\text{KSn}_2(\text{PO}_4)_3$ composite electrolyte from 300°C to 700°C as a function of temperature under dry nitrogen atmosphere are shown in Fig. 3. The results illustrate that the conductivities of pure $\text{Sn}_{0.9}\text{Mg}_{0.1}\text{P}_2\text{O}_7$ are similar to the previous experimental results of Tomita [11] under similar conditions. For the $\text{Sn}_{0.9}\text{Mg}_{0.1}\text{P}_2\text{O}_7/\text{KSn}_2(\text{PO}_4)_3$ composite, the conductivities increase with the increase of temperature and reach the highest conductivity of $6.3 \times 10^{-2} \text{ S}\cdot\text{cm}^{-1}$ at 700°C . To compare the conductivities of the $\text{Sn}_{0.9}\text{Mg}_{0.1}\text{P}_2\text{O}_7/\text{KSn}_2(\text{PO}_4)_3$ composite with other previous works, the results of

similar measurements on R^{n+} -doped $\text{Sn}_{1-x}\text{R}_x\text{P}_2\text{O}_7$ ($R = \text{Al}^{3+}$, In^{3+} and Mn^{2+}) [12,23-25] are also shown in Fig.3. Clearly, the $\text{Sn}_{0.9}\text{Mg}_{0.1}\text{P}_2\text{O}_7/\text{KSn}_2(\text{PO}_4)_3$ composite exhibits outstanding properties, the values of $\text{Sn}_{0.9}\text{Mg}_{0.1}\text{P}_2\text{O}_7/\text{KSn}_2(\text{PO}_4)_3$ are four to five orders of magnitude higher than those of $\text{Sn}_{0.9}\text{Mn}_{0.1}\text{P}_2\text{O}_7$ [12], $\text{Sn}_{0.9}\text{In}_{0.1}\text{P}_2\text{O}_7$ [24] and $\text{Sn}_{0.92}\text{In}_{0.08}\text{P}_2\text{O}_7$ [25], respectively. From these results, it can be concluded that the $\text{KSn}_2(\text{PO}_4)_3$ with a NASICON structure on the surface of $\text{Sn}_{0.9}\text{Mg}_{0.1}\text{P}_2\text{O}_7$ can provide additional transport pathways for protons and results in enhanced conductivities of the $\text{Sn}_{0.9}\text{Mg}_{0.1}\text{P}_2\text{O}_7/\text{KSn}_2(\text{PO}_4)_3$ composite, which is consistent with the results of XRD and SEM.

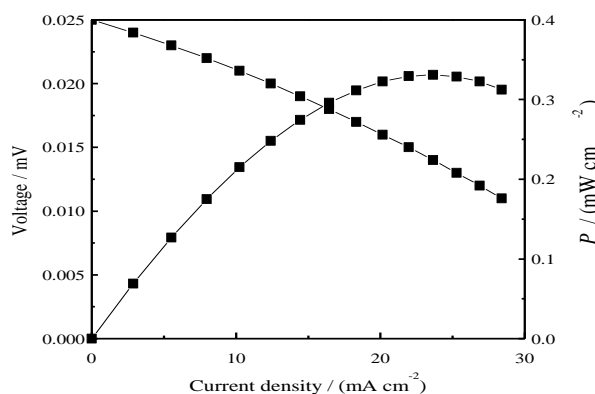


Figure 4. The oxygen concentration discharge cell: air, Pd-Ag | $\text{Sn}_{0.9}\text{Mg}_{0.1}\text{P}_2\text{O}_7/\text{KSn}_2(\text{PO}_4)_3$ | Pd-Ag, O_2 at 700 °C.

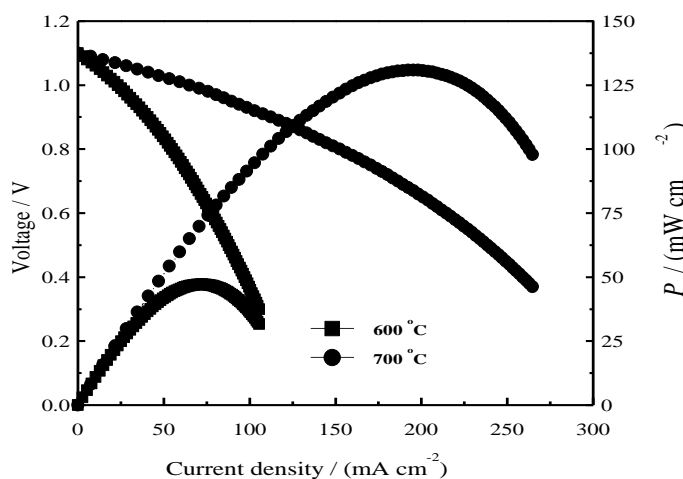


Figure 5. I-V-P curves of the H_2/O_2 fuel cell with the $\text{Sn}_{0.9}\text{Mg}_{0.1}\text{P}_2\text{O}_7/\text{KSn}_2(\text{PO}_4)_3$ at 600 °C and 700 °C.

To explore the oxide ionic conduction of the $\text{Sn}_{0.9}\text{Mg}_{0.1}\text{P}_2\text{O}_7/\text{KSn}_2(\text{PO}_4)_3$ composite in an oxygen-containing atmosphere, an oxygen concentration discharge cell was constructed at 700 °C and the results are shown in Fig.4. The theoretical electromotive forces (EMF_{cal}) of the oxygen concentration discharge cell can be calculated from $\text{EMF}_{\text{cal}} = \frac{RT}{4F} t_0 \ln[p_{\text{O}_2(\text{A})} / p_{\text{O}_2(\text{B})}]$ when $t_0 = 1$. The pure O_2 ($p_{\text{O}_2(\text{A})}$) and air ($p_{\text{O}_2(\text{B})}$) were passed into the cathode and anode chambers, respectively. From Fig.4, the measured open circuit voltage is 25 mV, which is lower than the theoretical calculated

EMF (32.7 mV). In addition, a stable discharge curve was observed. All the results demonstrate that the $\text{Sn}_{0.9}\text{Mg}_{0.1}\text{P}_2\text{O}_7/\text{KSn}_2(\text{PO}_4)_3$ composite has not only oxide ionic conduction but also a certain degree of electron hole conduction in an oxygen-containing atmosphere [26-27].

Fig. 5 displays the I - V - P curves of the H_2/O_2 fuel cell with the $\text{Sn}_{0.9}\text{Mg}_{0.1}\text{P}_2\text{O}_7/\text{KSn}_2(\text{PO}_4)_3$ composite electrolyte at 600 °C and 700 °C, respectively. It was found that the open circuit voltages are almost the same as the theoretical values, clearly demonstrating that the $\text{KSn}_2(\text{PO}_4)_3$ modified $\text{Sn}_{0.9}\text{Mg}_{0.1}\text{P}_2\text{O}_7$ composite electrolyte is sufficiently dense, in accordance with the TEM result. The maximum power output densities of the H_2/O_2 fuel cell are $47.2 \text{ mW}\cdot\text{cm}^{-2}$ at 600 °C and $130.9 \text{ mW}\cdot\text{cm}^{-2}$ at 700 °C, respectively. This good performance of the H_2/O_2 fuel cell using $\text{Sn}_{0.9}\text{Mg}_{0.1}\text{P}_2\text{O}_7/\text{KSn}_2(\text{PO}_4)_3$ composite electrolyte may rely on the dense composite frame which not only facilitate high ion transport but also increases the operation temperature range.

4. CONCLUSIONS

In this study, we have successfully synthesized a novel dense $\text{Sn}_{0.9}\text{Mg}_{0.1}\text{P}_2\text{O}_7/\text{KSn}_2(\text{PO}_4)_3$ composite electrolyte by using NaCl/KCl molten salt as the reaction medium as well as the reactant. The $\text{KSn}_2(\text{PO}_4)_3$ modified $\text{Sn}_{0.9}\text{Mg}_{0.1}\text{P}_2\text{O}_7$ composite exhibited markedly enhanced conductivities and the highest conductivity obtained was $6.3\times 10^{-2} \text{ S}\cdot\text{cm}^{-1}$ in a dry nitrogen atmosphere at 700 °C. The result of oxygen discharge concentration cell reveals that the composite has not only oxide ionic conduction but also a certain degree of electron hole conduction in an oxygen-containing atmosphere. It also displayed good fuel cell performances and the maximum power output densities were $47.2 \text{ mW}\cdot\text{cm}^{-2}$ at 600 °C and $130.9 \text{ mW}\cdot\text{cm}^{-2}$ at 700 °C.

ACKNOWLEDGEMENTS

This work was supported by the National Natural Science Foundation (No. 51402052, 21402029) of China. Horizontal cooperation project of Fuyang municipal government and Fuyang Normal College (No. XDHX2016019, XDHX2016002). Anhui Province Foundation (No. 1608085MB34, KJ2013Z266) of China, Excellent Youth Foundation of Anhui Educational Committee (gxyq2018046), and Excellent Youth Foundation of Fuyang Normal College (rcxm201805).

References

1. X.Y. Liu, Z.H. Xu and G.Y. Liang, *Mater. Lett.*, 191 (2017) 108.
2. H. Farnoush and Z. Rezaei, *Ceram. Int.*, 43 (2017) 11885.
3. V. N. Duy and H-M. Kim, *Int. J. Electrochem. Sci.*, 12 (2017) 11833.
4. L. Bi, E.H. Da'as and S.P. Shafi, *Electrochem. Commun.*, 80 (2017) 20.
5. X. Gao, J. Ma, Y. Li and H. Wei, *Int. J. Electrochem. Sci.*, 12 (2017) 11287.
6. K. K. Hansen, *Int. J. Electrochem. Sci.*, 12 (2017) 11540.
7. J. Luo, A.H. Jensen, N.R. Brooks, J. Sniekers, M. Knipper, D. Aili, Q. Li, B. Vanroy, M. Wübbenhorst, F. Yan, L.V. Meervelt, Z. Shao, J. Fang, Z.-H. Luo, D.E.D. Vos, K. Binnemans and J. Fransaer, *Energy Environ. Sci.*, 8(2015) 1276.

8. G. Almutairi¹, F. Alenazey, Y. Yousef and B. Alshammari, *Int. J. Electrochem. Sci.*, 12 (2017) 11616.
9. A.M. Abdalla, S. Hossain, A.T. Azad, P.M.I. Petra, F. Begum, S.G. Eriksson and A.K. Azad, *Renew. Sust. Energ. Rev.*, 82 (2018) 353.
10. O. K. Alekseeva, E. K. Lutikova, V. V. Markelov, V. I. Porembsky and V. N. Fateev, *Int. J. Electrochem. Sci.*, 13 (2018) 797.
11. A. Tomita, N. Kajiyama, T. Kamiya, M. Nagao and T. Hibino, *J. Electrochem. Soc.*, 154 (2007) B1265.
12. B. Singh, J.H. Kim, O. Parkash and S.J. Song, *Ceram. Int.*, 42 (2016) 2983.
13. M. Nagao, T. Kamiya, P. Heo, A. Tomita, T. Hibino and M. Sano, *J. Electrochem. Soc.*, 153 (2006) A1604.
14. Y.C. Jin and T. Hibino, *Electrochim. Acta*, 55 (2010) 8371.
15. Y. Sato, Y.B. Shen, M. Nishida, W. Kanematsu and T. Hibino, *J. Mater. Chem.*, 22 (2012) 3973.
16. P. Heo, Y. Shen, K. Kojima, C. Pak, K.H. Choi and T. Hibino, *Electrochim. Acta*, 128 (2014) 287.
17. J. Liao, J. Yang, Q. Li, L.N. Cleemann, J.O. Jensen, N.J. Bjerrum, R. He and W. Xing, *J. Power Sources*, 238 (2013) 516.
18. J. Han, M. Xu, Y. Niu, M. Jia, T. Liu, C and M. Li, *J. Colloid Interf. Sci.*, 483 (2016) 67.
19. N. Li, Y. Wang, R. Rao, X. Dong, X. Zhang and S. Zhu, *Appl. Surf. Sci.*, 399 (2017) 624.
20. A.I. Mohamed and J.F. Whitacre, *Electrochim. Acta*, 235 (2017) 730.
21. P. Hu, J. Ma and T. Wang, *Chem. Mater.*, 27 (2015) 6668.
22. J. Liu, R. Du, R. Shi and H. Wang, *Ceram. Int.*, 44 (2018) 5179.
23. H Wang, L Sun, J Chen and C Luo, *Acta Phys.-Chim. Sin.*, 28 (2012) 2893.
24. S.R. Phadke, C.R. Bowers, E.D. Wachsman and J.C. Nino, *Solid State Ion.*, 183 (2011) 26.
25. S. Tao, *Solid State Ion.*, 180 (2009) 148.
26. J. Guan, S.E. Dorris, U. Balachandran and M. Liu, *Solid State Ion.*, 100 (1997) 45.
27. G. Ma, T. Shimura and H. Iwahara, *Solid State Ion.*, 120 (1999) 51.

© 2018 The Authors. Published by ESG (www.electrochemsci.org). This article is an open access article distributed under the terms and conditions of the Creative Commons Attribution license (<http://creativecommons.org/licenses/by/4.0/>).